Synthesize of GaN/quartz Nanostructure Using Pulsed Laser Ablation in Liquid for Optoelectronic Devices

Husam Aldin A. Abdul Amir
University of Technology-Iraq
Makram A Fakhri (mokaram_76@yahoo.com)
University of Technology-Iraq https://orcid.org/0000-0001-9010-6121
Ali. A. Alwahib
University of Technology-Iraq
Evan T. Salim
University of Technology-Iraq

Research Article

Keywords: Gallium nitride, Deposition by pulse laser ablation, X-Ray Diffraction (XRD), TEM, AFM, FESEM, PL

Posted Date: August 4th, 2021

DOI: https://doi.org/10.21203/rs.3.rs-772378/v1

Abstract

This study involves synthesizing gallium nitride (GaN) nanoparticles (NPs) under six different ablation energies using the pulsed laser ablation method. The nanoparticle was deposited using drop cast method on a quartz substrate. XRD pattern shows two peaks of h-GaN nanoparticles at 2θ = 34.64 and 37.98, reflected from (002) and (100) planes. The morphological properties indicate the hexagonal crystal nature of GaN that shows in the XRD pattern. Photoluminescence (PL) spectra show the highest laser power, 2000 mj has a minor emission peaked at 3.34 eV. The maximum emission peak 3.83 eV at 1400 mJ. The study depends on the pulsed laser to generate nanoparticles with different characteristics.

Introduction

Advanced electronic systems have been applied in optical devices depending on significant work that has been done for decades on large bandgap materials. These devices can typically be controlled at higher temperatures, higher voltages, and higher power densities, making them extremely interesting for future electronic systems[1, 2].

Due to its direct-wide band gap (3.4eV) and high thermal conductivity [3-7], thermal stability, high melting point [8], high electron mobility [9], mechanical hardness, and high breakdown voltage [10], the material gallium nitride (GaN) has become more attractive in recent years. Due to these properties, thin film has become one of the essential materials of industrial devices.

Gallium nitride (GaN) high thermal conductivity material that makes it ideal for use in different sensors applications [11-28], solar cells [19, 20], light-emitting diode devices [21-23], short wavelength optical devices [24], high-power transistors [25, 26], and beta-voltaic devices [27].

Several studies have attempted to synthesize GaN nanostructures using various growth techniques, including metal-organic chemical vapor deposition[28, 29], reactive molecular beam epitaxy [30], thermal ammonization [31], physical vapor deposition [32], chemical vapor deposition (CVD) [33, 34], sol-gel chemistry [35], electrochemical deposition [36], thermal vapor deposition [37], and combust vapor deposition[38-40]. These methods have a common drawback in high temperatures and costly chemicals, leading to a relatively low production yield. Therefore, pulsed laser deposition (PLD) [41] has recently improved the high quality of GaN films. This technique has been commonly used in the past to prepare thin films for high-quality multicomponent oxide ceramics. PLD is a perfect growth approach with many benefits over other methods, such as being very easy to operate, having no toxic or costly precursors, and thin film can be achieved at relatively low temperatures [42, 43].

In this research involves synthesizing high-quality gallium nitride (GaN) nanoparticles (NPs) under six different ablation energies using the pulsed laser ablation method and deposited on the quartz substrates for fabricating high-quality optoelectronic devices and gas sensors.

Experimental Detail

In this experiment, The GaN target was submerged in 5ml ethanol and fired using the pulsed laser Nd: YAG, as shown in Figure 1 (a). The laser parameters were correctly indicated by the frequency and wavelength (532nm) (4 Hz). For each flow energy of 1000 mJ, 1200 mJ, 1400 mJ, 1600 mJ, 1800 mJ, and 2000 mJ, six samples were prepared. With 500 pulses, each piece was irradiated to saturate the liquid with nanomaterials. After every 100 pulses, the focal length varied by 12 cm to retain the laser and the GaN surface contact in the same way. Figure 1(b) shows the liquid sample after the Nd: YAG pulsed laser ablation phase.

As shown in Figure 2, the GaN liquid samples were deposited onto the quartz substrate using a drop-casting process. A hotplate heated the quartz layer at a range of temperatures from (70^{o}C -90^{o}C). When the appropriate temperature was reached, nano-liquid was slowly dropped on the quartz substrate; each drop on the quartz substrate was left to dry and then followed by another drop (100 drops) to form the thin film GaN on the quartz substrate. The processes were performed in less than 12 hours to prevent oxidation during deposition. Before beginning the falling process with alcohol, the quartz substrate was thoroughly washed. Before each drop, the nano-liquid should be sufficiently shaken to preserve the GaN nanomaterials.

The quartz/nanoparticles (GaN) sample was tested in the XRD test, TEM, AFM, FESEM, PL. All results are analyzed in the next section of results and discussions.

Results And Discussion

3-1- Structural properties

Fig. 3 presents the XRD GaN nanoparticles synthesized and drop-casted on quartz substrate at different ablation energies (1000, 1200, 1400, 1600, 1800, and 2000mj). The diffraction peaks in the XRD pattern are matched with standard cubic and wurtzite hexagonal structures of the GaN crystal. The nanoparticles prepared for 1000mj exhibit h-GaN rise at 2θ =34.64 reflected from (002) plane and c-GaN peak at 2θ =40.22 reflected from (111) plane cubic phase has affected the peak intensity and the sharpness of the hexagonal phase. The sample of 1200mj displays h-GaN nanoparticles at 2θ = 34.64 and 37.98, which are reflected from (002) and (100) planes. The intensity and the sharpness of the peak begin to increase with increasing the ablation energy. The third sample of 1400mj shows two peaks of h-GaN nanoparticles at 2θ = 34.64, and 37.98 reflected from (002) and (100) planes, the intensity of the peak increased due to increase the structure crystallization. The fourth sample of 1600mj displays h-GaN nanoparticles at 2θ = 34.64 and 37.98, which is reflected from (002) and (100) planes; this sample has the highest peak due to the excellent quality of h-GaN nanoparticles. The fifth sample of 1800mj shows two peaks of h-GaN nanoparticles at 2θ = 34.64 and 37.98, which reflected from (002) and (100) planes, the peak intensity begins to decrease due to decreasing the structure crystallization, and the sixth sample of 2000 mJ shows two peaks of h-GaN nanoparticles at 2θ = 34.64 and 37.98 which reflected from (002) and (100) planes, the intensity of the peak is less than the fifth sample. This indicates high intensity in response to the excellent quality of h-GaN nanoparticles synthesized in the fourth sample at low temperature.

Furthermore, it is shown that the intensity of the peaks for the XRD pattern increased with increasing laser ablation energy due to increasing of the grain size and concentration of ablated material and due to enhancement of crystal quality until (1600 mJ) that has the highest intensity peak then the intensity peak back to decrease as the laser ablation increase.

3-2- Morphological properties

3-2-1 AFM results

This section includes a profound discussion of the results. Fig.4 presents AFM images of the GaN nanophotonic; the thickness of the outer layer affected by the laser ablation energy where at 1000 mJ the thickness was 37 nm and increase at 1200 mJ to be 40 nm and then decrease at 1400 mJ and 1600 mJ that have the less thickness than other due to high regular crystals distribution and the small rang of grain size and then back to increase at 1800 mJ with 62nm because of the decrease in the regularity of the distribution of the crystal and then back to decrease at 2000 mJ to be 27 nm due to regular crystals distribution [44].

Fig. 5 presents the change in the root mean square and roughness and grain size of the GaN nanophotonic, with the difference in the pulsed laser ablation energy. The GaN nanoparticles prepared for 1000mj exhibit high root mean square (23.40nm) and roughness (3.750nm). The sample of 1200 mJ displays root mean square (16.00nm) and roughness of (4.533nm). The sample of 1400mj and 1600mj shows the highest roughness .The smallest root mean square due to the excellent quality of the structure crystallization and high regular crystals distribution, the roughness back to decrease, and the root mean square increase cause the reduction in the structure crystallization and regular crystals distribution 1800 mJ and 2000mJ [44].

Fig. 6 represents the relation between the grains density and the grains size at different ablation energies. The GaN nanoparticles prepared for 1000mj exhibit a wide range of grain size (27. 29 nm - 116.6nm) with grains density (0.002). The sample 1200 mJ display a range of grain size (12.57 nm-103.7nm), the range of grain size decrease and the grains density increase. The samples of 1400 mJ and1600 mJ show the smallest range of grain size (4.361nm-58.88nm) and (9.183nm-69.44nm) and the highest grains density due to high regular crystals distribution, then the density of the grain back to decrease at 1800 mJ because of the decrease in the regularity of the distribution of the crystal and then back to increase at 2000 mJ due to regular crystals distribution [45].

Fig. 7 presents frequency with the grain size of GaN/quartz nanostructures at different ablation energies. The surface topography of GaN nanophotonic as observed from the AFM micrographs proves that the grains are uniformly distributed within the scanning area (78nm × 78nm), with individual columnar grains extending upward. This surface characteristic is quoted from the topographic image, which is uniform, smooth and homogeneous at 1400 mJ. The third sample of 1400 mJ has Gaussian distribution due to the excellent quality of the structure crystallization. The fourth sample of 1600 mJ

also has Gaussian distribution with a broader scope than (1400 mJ) sample. Other samples show the ununiform distribution of particle size, which leed to optical and electrical properties inhomogeneous.

3-2-2 FESEM results

Fig. 8 presents the FESEM images and the EDX spectrum of GaN nanoparticles for the six samples synthesized under different ablation energies. These samples were built using a drop cast on the quartz substrate. The EDX spectra of GaN nanoparticles have both elements Ga, and N. The [Ga]/N ratio depends on laser ablation energy. At 1000 mJ, FESEM image shows the beginning of the crystallization process, and the ratio of [Ga] / [N] was 5. The second sample at 1200 mJ exhibits an increase in the structure crystallization. The ratio of [Ga] / [N] was 3.77. The third sample of 1400 mJ shows improves crystallization than the second sample; the ratio of [Ga] / [N] was 3.633. The fourth sample at 1600 mJ shows a good crystallization quality, the ratio of [Ga] / [N] was 4.19. The fifth sample at 1800 mJ exhibits several particles to be agglomerated; the ratio of [Ga] / [N] was 3. The sixth sample at 2000 mJ shows an increase in the number of agglomerated particles with increasing the laser ablation energy, the ratio of [Ga] / [N] was 3.45.

Moreover, FESEM images showed that the crystallization of GaN nanoparticle increased with increasing laser ablation energy due to increased grain size, the concentration of ablated material becoming higher, and the enhancement of crystal quality until (1600 mJ), and this in good agreement with XRD result. Increasing the laser ablation energy above 1600 mJ will make the particles agglomerated, and the number of agglomerated particles will increase with increasing the laser ablation energy.

3-2-3 TEM results

TEM was performed to obtain a submicroscopic image of the nanoparticles of less than 100nm. Fig.9a shows the 1000 mJ indicates that the GaN nanoparticles have quasi-spherical particles with grain size varies from 27.29nm to116.6nm. Fig.9b at 1000 mJ, the sample exhibited a good crystallization quality with the lowest grain size ranging from 4.361nm to 58.88nm. Fig.9c prepared for 1800 mJ shows grain size varies from 4.196nm to 88.51nm; the particles began to agglomerate with increasing the laser ablation energy. The TEM images support the FESEM images of GaN. The FESEM with EDX and TEM also validated the GaN nanoparticles' chemical purity earlier shown with the XRD data. Therefore, it can be inferred that ablation energy is crucial in the synthesis GaN nanoparticles.

3-3- Optical properties

Fig. 10 demonstrates the photoluminescence (PL) spectra of the prepared GaN under different laser ablation energies. The energy of the incident photon ( ) as a function of the wavelength (λ) was calculated using equation (1)

$$Eg = \frac{1240}{\lambda} \qquad (1)$$

The first GaN nanoparticle prepared for 1000 mJ presents an energy gap of 3.38 eV at the wavelength 366nm. The second sample prepared for 1200mj exhibits an energy gap of 3.41 eV at the wavelength 363nm. The energy gap increases with increasing the ablation energy, and the wavelength will have a blue shift. The third sample prepared for 1400 mJ presents an energy gap of 3.83 eV at the wavelength 323 nm; this sample has the highest energy gap due to the small piratical size and the blue shift. The fourth sample prepared for 1600 mJ exhibits an energy gap of 3.71 eV at 334 nm. The energy gap began to decrease with increasing the ablation energy that will ablate large piratical size, and the wavelength will have redshift. The fifth sample prepared for 1800 mJ exhibit an energy gap of 3.54 eV at the wavelength 350 nm; the wavelength will have a redshift, and the energy gap decrease. The sixth sample prepared for 2000mj present the smallest energy gap of 3.34 eV at the wavelength 371nm; the wavelength will have redshift, the photoluminescence (PL) investigation proved the AFM result.

Furthermore, It can be seen that increasing the ablation energy will remove the larger particle size, and therefore, the wavelength will have a red shift, So decreasing the ablation energy will make a blue shift in the wavelength and increase the energy gap until 1400mj that has the highest peak of power then at 1200 and 1000 mJ the energy gap decrease and wavelength will have redshift due to the core-shell phenomenon.

Conclusion

This paper presents the synthesis of gallium nitride (GaN) nanoparticles (NPs) under six different ablation energies using pulsed laser ablation method. GaN deposited on the quartz substrate analyzed using XRD, AFM, FESEM, TEM, and PL tests. XRD test indicates high intensity in response to the excellent quality of h-GaN nanoparticles synthesized in the fourth sample. The morphological properties (AFM, FESEM, and TEM) inferred that ablation energy is a critical factor in the synthesis GaN nanoparticles. Photoluminescence (PL) spectra proved that decreasing the ablation energy will make a blue shift in the wavelength and increase the energy gap until 1400 mJ, the highest peak of energy at 1400 mJ. The energy gap decrease and wavelength will have redshift due to the core-shell phenomenon.

References

1. L. Sang, M. Liao, M. Sumiya, A comprehensive review of semiconductor ultraviolet photodetectors: from thin film to one-dimensional nanostructures. Sensors **13**(8), 10482–10518 (2013)
2. R. Velazquez, A. Aldalbahi, M. Rivera, P. Feng, Fabrications and application of single crystalline GaN for high-performance deep UV photodetectors. AIP Adv. **6**(8), 85117 (2016)
3. H. Qiu, C. Cao, H. Zhu, Synthesis of nanocrystalline GaN by the sol–gel method. Mater. Sci. Eng. B **136**(1), 33–36 (2007)
4. G. Sinha, K. Adhikary, S. Chaudhuri, Synthesis and optical characterization of c-axis oriented GaN thin films on amorphous quartz glass via sol–gel process. Appl. Surf. Sci. **254**(16), 5257–5260 (2008)

5. K. Sardar, A.R. Raju, G.N. Subbanna, Epitaxial GaN films deposited on sapphire substrates prepared by the sol–gel method. Solid State Commun. **125**(6), 355–358 (2003)
6. A. Majid et al., Optical, electronic and magnetic properties of Cr: GaN thin films. Mater. Chem. Phys. **136**, no. 2–3 (2012), "," , , pp. 809–815
7. D.-W. Kang, J.-Y. Kwon, J. Shim, H.-M. Lee, M.-K. Han, Highly conductive GaN anti-reflection layer at transparent conducting oxide/Si interface for silicon thin film solar cells. Sol. energy Mater. Sol. cells **105**, 317–321 (2012)
8. A. Mantarcı, Structural, Morphological, and Optical Characterization of GaN/p-Si Thin Films for Various Argon Flow Rates. JOM **72**(1), 552–560 (2020)
9. X.G. He et al., GaN high electron mobility transistors with AlInN back barriers. J. Alloys Compd. **662**, 16–19 (2016)
10. W. Saito, T. Suwa, T. Uchihara, T. Naka, T. Kobayashi, Breakdown behaviour of high-voltage GaN-HEMTs. Microelectron. Reliab. **55**, no. 9–10 (2015), "," , , pp. 1682–1686
11. M.S.Z. Abidin, H.A.M. Shahjahan, A.M. Hashim, Surface reaction of undoped AlGaN/GaN HEMT based two terminal device in H + and OH-ion-contained aqueous solution. Sains Malaysiana **2**, 197–203 (2013)
12. M.S.Z. Abidin, A.M. Hashim, M.E. Sharifabad, S.F.A. Rahman, T. Sadoh, Open-gated pH sensor fabricated on an undoped-AlGaN/GaN HEMT structure. Sensors **11**(3), 3067–3077 (2011)
13. M. Mohamad et al., "The sensing performance of hydrogen gas sensor utilizing undoped-AlGaN/GaN HEMT," in *2010 IEEE International Conference on Semiconductor Electronics (ICSE2010)*, 2010, pp. 301–304
14. S.J. Pearton, F. Ren, Gallium nitride-based gas, chemical and biomedical sensors. IEEE Instrum. Meas. Mag. **15**(1), 16–21 (2012)
15. B.H. Chu et al., Aluminum gallium nitride (GaN)/GaN high electron mobility transistor-based sensors for glucose detection in exhaled breath condensate. J. Diabetes Sci. Technol. **4**(1), 171–179 (2010)
16. B. Chitara, D.J. Late, S.B. Krupanidhi, C.N.R. Rao, Room-temperature gas sensors based on gallium nitride nanoparticles. Solid State Commun. **150**, no. 41–42 (2010), "," , , pp. 2053–2056
17. J. Schalwig, G. Müller, O. Ambacher, M. Stutzmann, Group-III-Nitride Based Gas Sensing Devices. Phys. status solidi **185**(1), 39–45 (2001)
18. D.-S. Lee, J.-H. Lee, Y.-H. Lee, D.-D. Lee, GaN thin films as gas sensors. Sensors Actuators B Chem. **89**(3), 305–310 (2003)
19. M. Miyoshi, T. Tsutsumi, T. Kabata, T. Mori, T. Egawa, Effect of well layer thickness on quantum and energy conversion efficiencies for InGaN/GaN multiple quantum well solar cells. Solid State Electron. **129**, 29–34 (2017)
20. J.-K. Sheu, P.-C. Chen, C.-L. Shin, M.-L. Lee, P.-H. Liao, W.-C. Lai, Manganese-doped AlGaN/GaN heterojunction solar cells with intermediate band absorption. Sol. Energy Mater. Sol. Cells **157**, 727–732 (2016)

21. Z. Liu, W.C. Chong, K.M. Wong, K.M. Lau, GaN-based LED micro-displays for wearable applications. Microelectron. Eng. **148**, 98–103 (2015)
22. J.-H. Lin, S.-J. Huang, Y.-K. Su, K.-W. Huang, The improvement of GaN-based LED grown on concave nano-pattern sapphire substrate with SiO2 blocking layer. Appl. Surf. Sci. **354**, 168–172 (2015)
23. A. Mantarcı, B. Gündüz, A study on refractive index dispersion and optoelectronic parameters of the BCzVB OLED material by using solution method. Opt. Quantum Electron. **48**(12), 547 (2016)
24. E. Martínez-Guerrero et al., Self-assembled zinc blende GaN quantum dots grown by molecular-beam epitaxy. Appl. Phys. Lett. **77**(6), 809–811 (2000)
25. J.-M. Lee, B.-G. Min, C.-W. Ju, H.-K. Ahn, J.-W. Lim, High temperature storage test and its effect on the thermal stability and electrical characteristics of AlGaN/GaN high electron mobility transistors. Curr. Appl. Phys. **17**(2), 157–161 (2017)
26. H. Qian et al., Novel GaN-based vertical heterostructure field effect transistor structures using crystallographic KOH etching and overgrowth. J. Cryst. Growth **459**, 185–188 (2017)
27. M.R. Khan et al., Design and characterization of GaN pin diodes for betavoltaic devices. Solid State Electron. **136**, 24–29 (2017)
28. W.-G. Jung, S.-H. Jung, P. Kung, M. Razeghi, Fabrication of GaN nanotubular material using MOCVD with an aluminium oxide membrane. Nanotechnology **17**(1), 54 (2005)
29. C. Saidi, N. Chaaben, A. Bchetnia, A. Fouzri, N. Sakly, B.El Jani, Growth of scandium doped GaN by MOVPE. Superlattices Microstruct. **60**, 120–128 (2013)
30. Y.S. Park, T.W. Kang, R.A. Taylor, Abnormal photoluminescence properties of GaN nanorods grown on Si (111) by molecular-beam epitaxy. Nanotechnology **19**(47), 475402 (2008)
31. S. Xue, X. Zhang, R. Huang, D. Tian, H. Zhuang, C. Xue, A simple method for the growth of high-quality GaN nanobelts. Mater. Lett. **62**, no. 17–18 (2008), “,”, , pp. 2743–2745
32. K.M.A. Saron, M.R. Hashim, Broad visible emission from GaN nanowires grown on n-Si (1 1 1) substrate by PVD for solar cell application. Superlattices Microstruct. **56**, 55–63 (2013)
33. Y.B. Tang et al., Vertically aligned p-type single-crystalline GaN nanorod arrays on n-type Si for heterojunction photovoltaic cells. Nano Lett. **8**(12), 4191–4195 (2008)
34. Q.N. Abdullah, F.K. Yam, J.J. Hassan, C.W. Chin, Z. Hassan, M. Bououdina, High performance room temperature GaN-nanowires hydrogen gas sensor fabricated by chemical vapor deposition (CVD) technique. Int. J. Hydrogen Energy **38**(32), 14085–14101 (2013)
35. A. Podhorodecki, M. Nyk, R. Kudrawiec, J. Misiewicz, J.C. Pivin, W. Strek, Optical properties of GaN nanocrystals embedded into silica matrices. Superlattices Microstruct. **40**, no. 4–6 (2006), “,”, , pp. 533–536
36. K. Al-Heuseen, M.R. Hashim, N.K. Ali, Synthesis of hexagonal and cubic GaN thin film on Si (111) using a low-cost electrochemical deposition technique. Mater. Lett. **64**(14), 1604–1606 (2010)
37. Y. Tokuda, Y. Matsuoka, H. Ueda, O. Ishiguro, N. Soejima, T. Kachi, DLTS study of n-type GaN grown by MOCVD on GaN substrates. Superlattices Microstruct. **40**, no. 4–6 (2006), “,”, , pp. 268–273

38. O.I. Mićić, S.P. Ahrenkiel, D. Bertram, and and A.J. Nozik, Synthesis, structure, and optical properties of colloidal GaN quantum dots. Appl. Phys. Lett. **75**(4), 478–480 (1999)
39. T.-J. Kuo, C.-L. Kuo, C.-H. Kuo, M.H. Huang, Growth of Core – Shell Ga – GaN Nanostructures via a Conventional Reflux Method and the Formation of Hollow GaN Spheres. J. Phys. Chem. C **113**(9), 3625–3630 (2009)
40. K.M.A. Saron, M.R. Hashim, Study of using aqueous NH3 to synthesize GaN nanowires on Si (1 1 1) by thermal chemical vapor deposition. Mater. Sci. Eng. B **178**(5), 330–335 (2013)
41. M. Cazzanelli et al., Luminescent properties of GaN thin films prepared by pulsed laser deposition. Mater. Sci. Eng. B **59**, no. 1–3 (1999), "," , , pp. 137–140
42. Z.E. SLAIBY, A. RAMIZY, "SYNTHESIS GALLIUM NITRIDE THIN FILMS BY, PULSED LASER DEPOSITION AS AMMONIA (NH, 3) GAS SENSOR. J. Optoelectron. Biomed. Mater. Vol **12**(1), 17–23 (2020)
43. B.Y. Man et al., Effects of ZnO buffer layers on the fabrication of GaN films using pulsed laser deposition. J. Appl. Phys. **101**(9), 93519 (2007)
44. G.S. Sudhir et al., Control of the structure and surface morphology of gallium nitride and aluminum nitride thin films by nitrogen background pressure in pulsed laser deposition. J. Electron. Mater. **27**(4), 215–221 (1998)
45. A. Mantarcı, Structural, Morphological, and Optical Characterization of GaN/p-Si Thin Films for Various Argon Flow Rates. JOM **72**(1), 552–560 (2020)

Figures

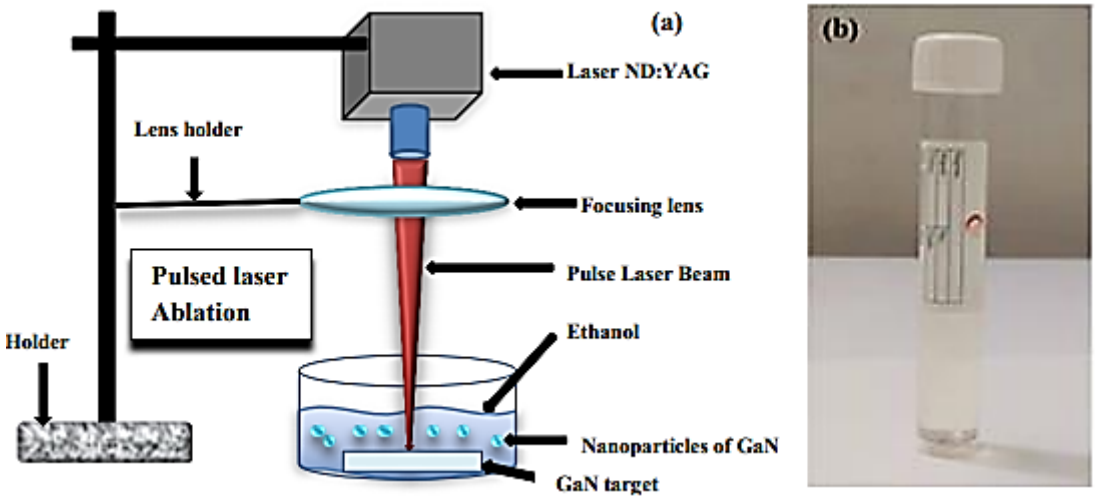

Figure 1

a) laser ablation method b) liquid sample generated from ablation method

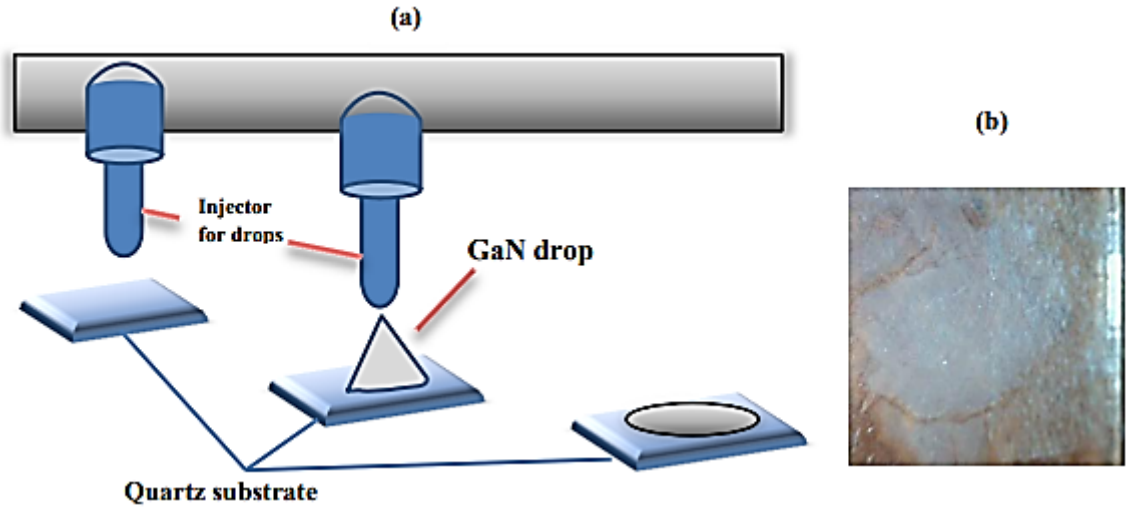

Figure 2

a) drop-casting method for GaN b) GaN/Quartz thin film

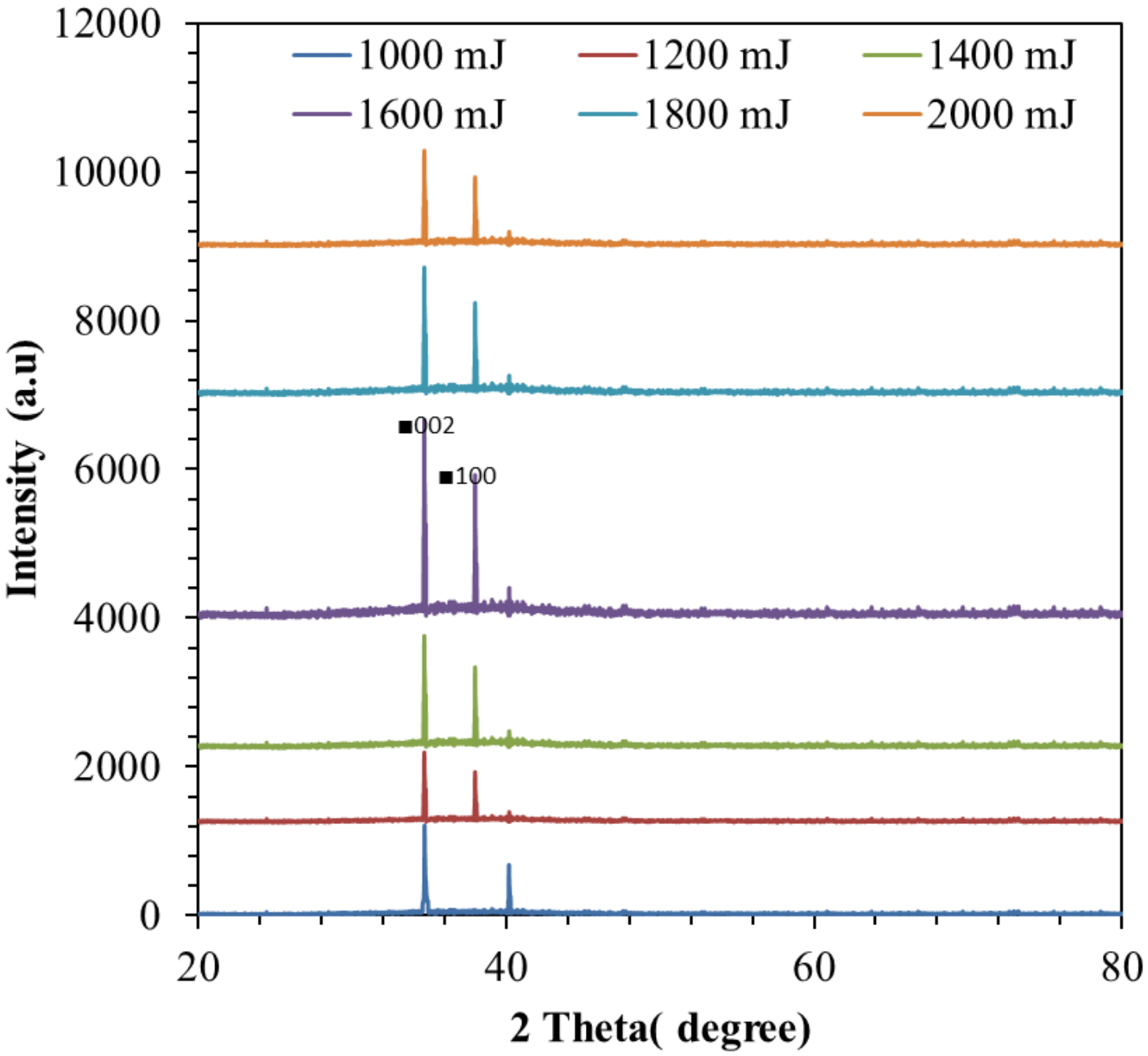

Figure 3

XRD patterns of GaN nanophotonic with different ablation energies

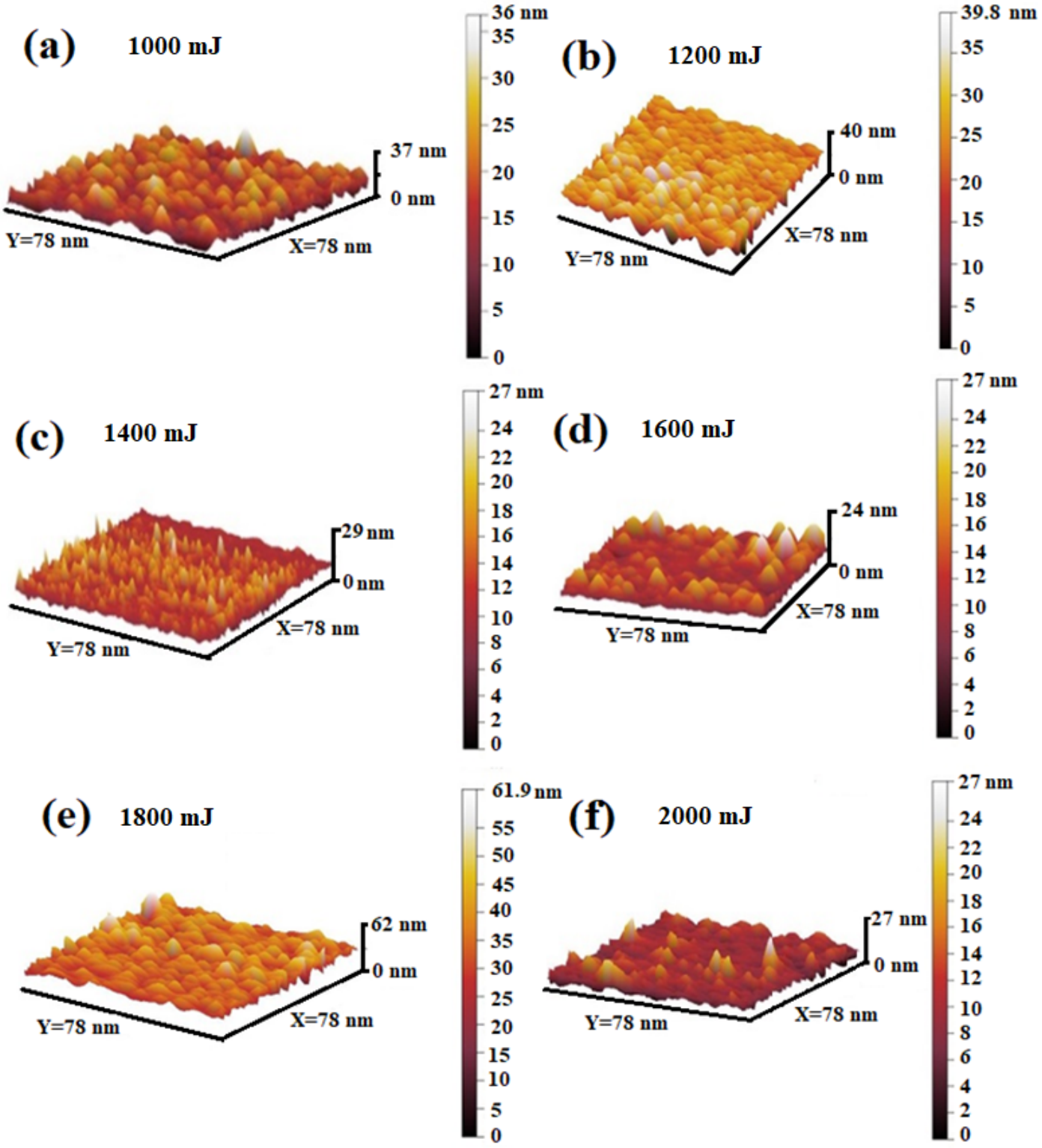

Figure 4

AFM images of GaN/quartz nanostructures at different ablation energies

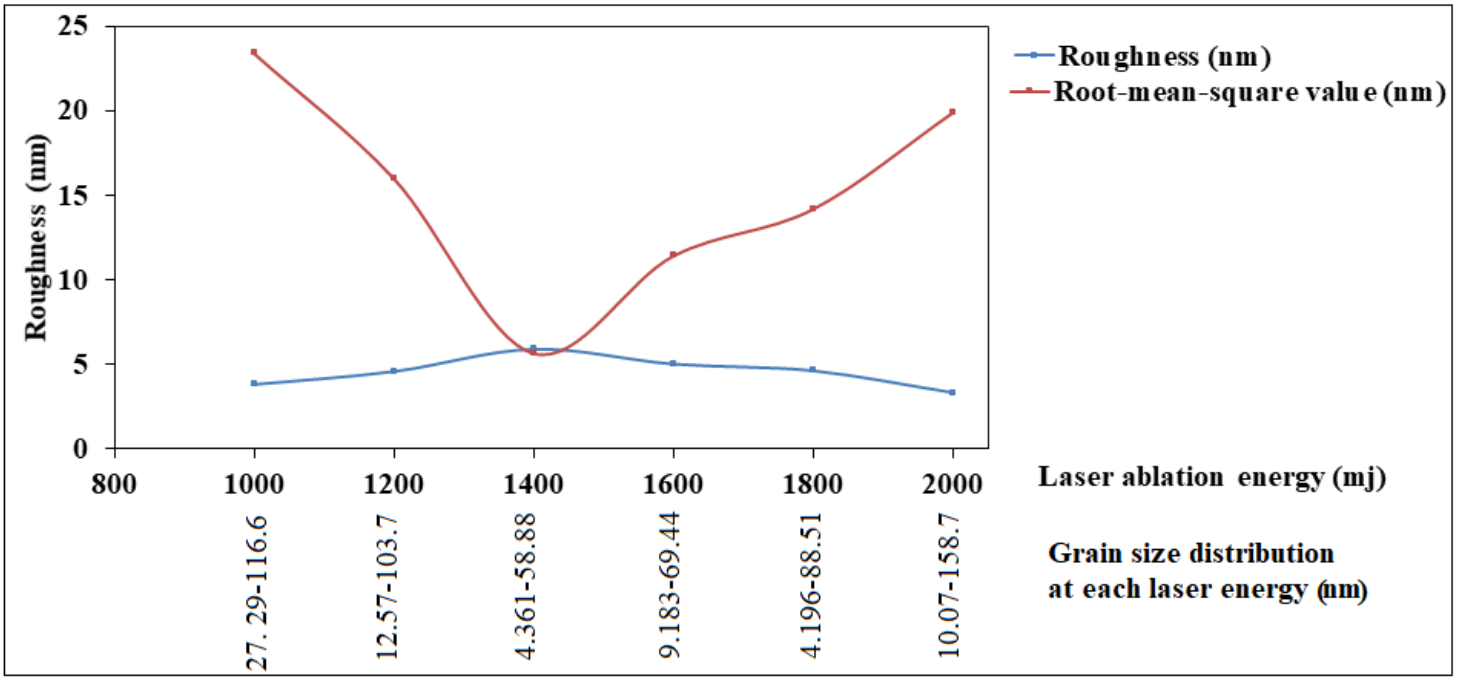

Figure 5

The roughness of GaN/quartz nanostructures at different ablation energies.

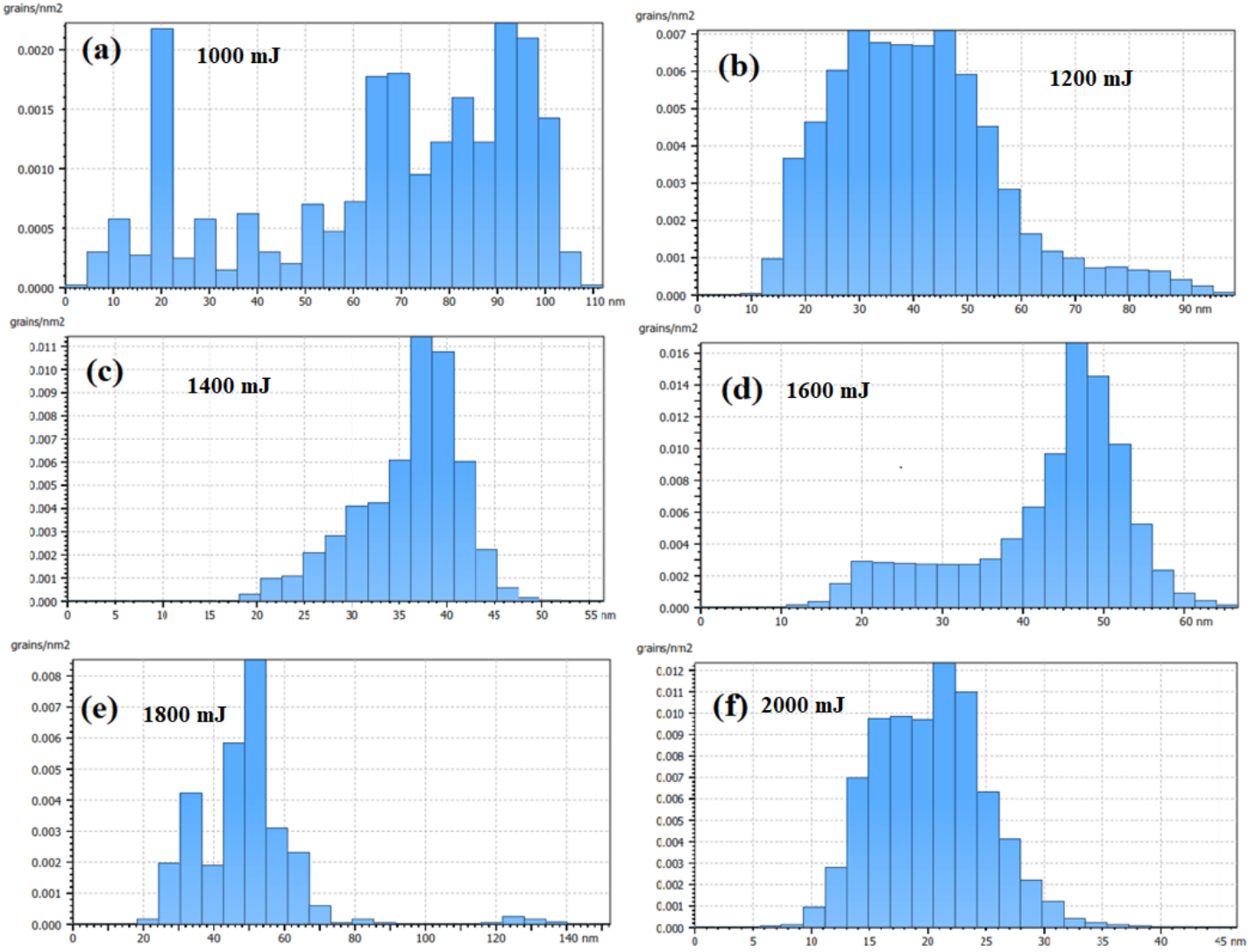

Figure 6

The average grain size curve of GaN/quartz nanostructures at different ablation energies

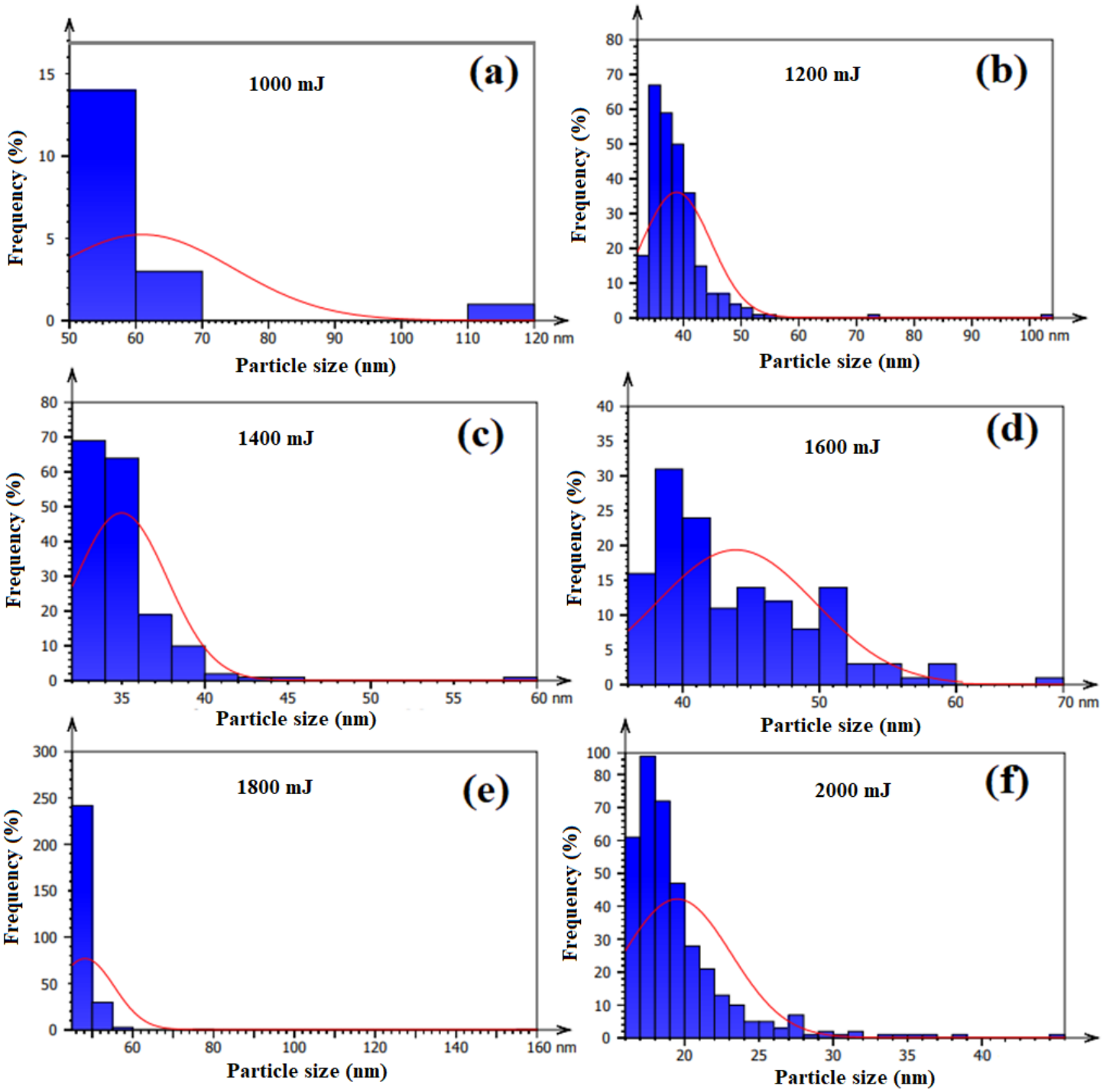

Figure 7

Number of the frequency with the grain size of GaN/quartz nanostructures at different ablation energies

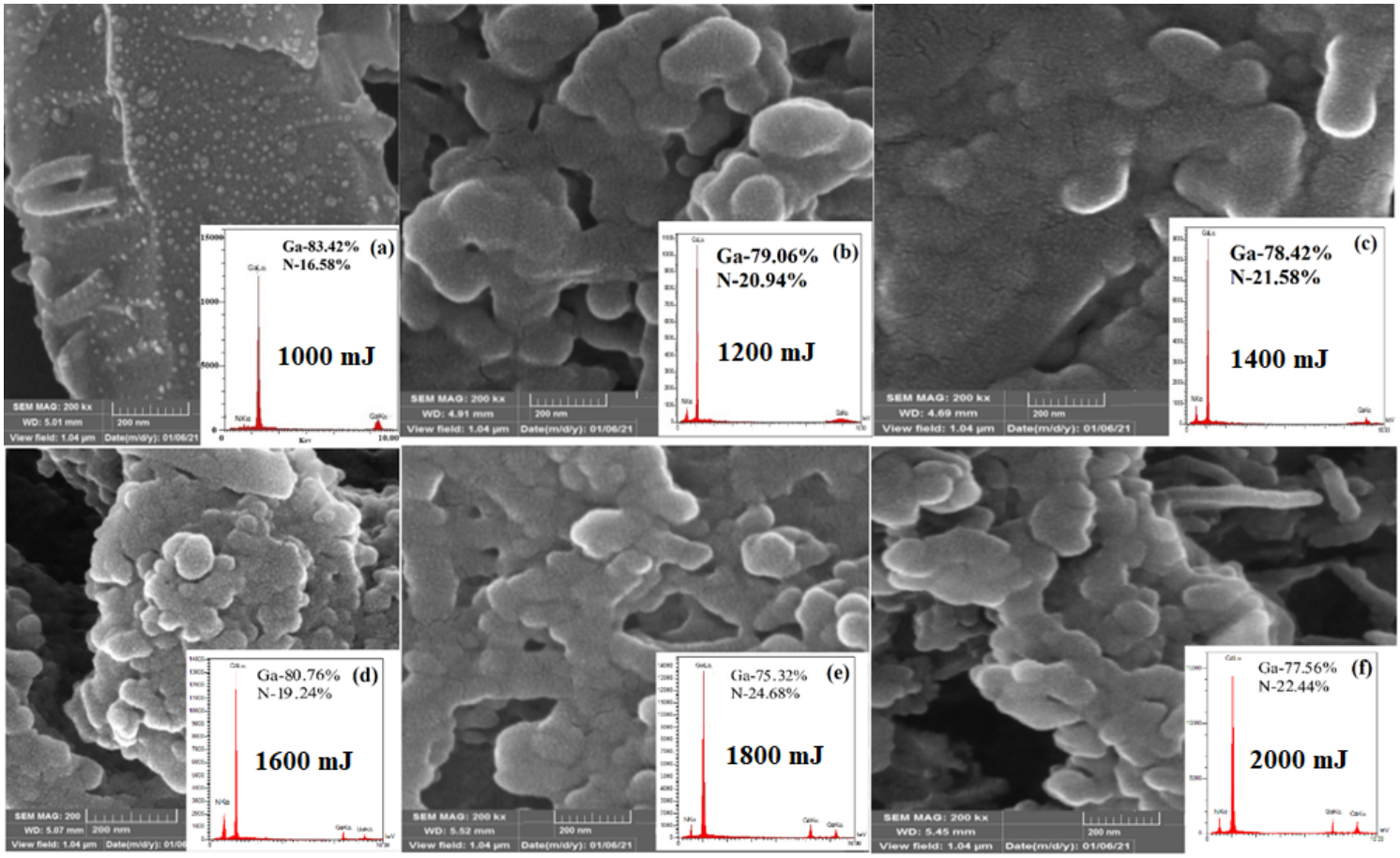

Figure 8

The FESEM images and EDX spectra of the GaN nanostructures grown on the quartz substrates at different ablation energies

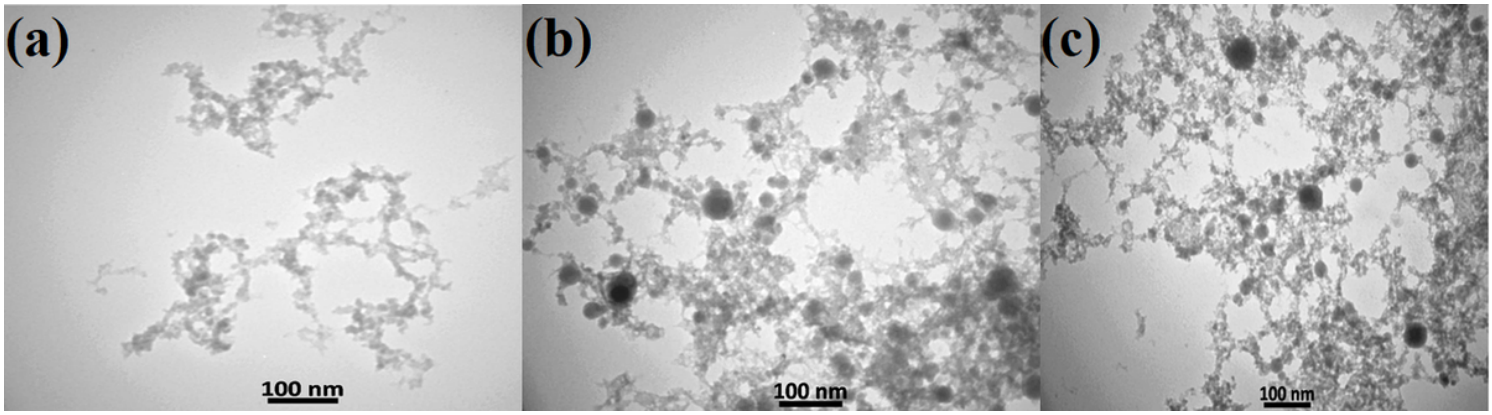

Figure 9

TEM images of the GaN nanostructures grown on the quartz substrates at different ablation energies (a) 1000 mJ, (b) 1400 mJ, and (c) 1800 mJ

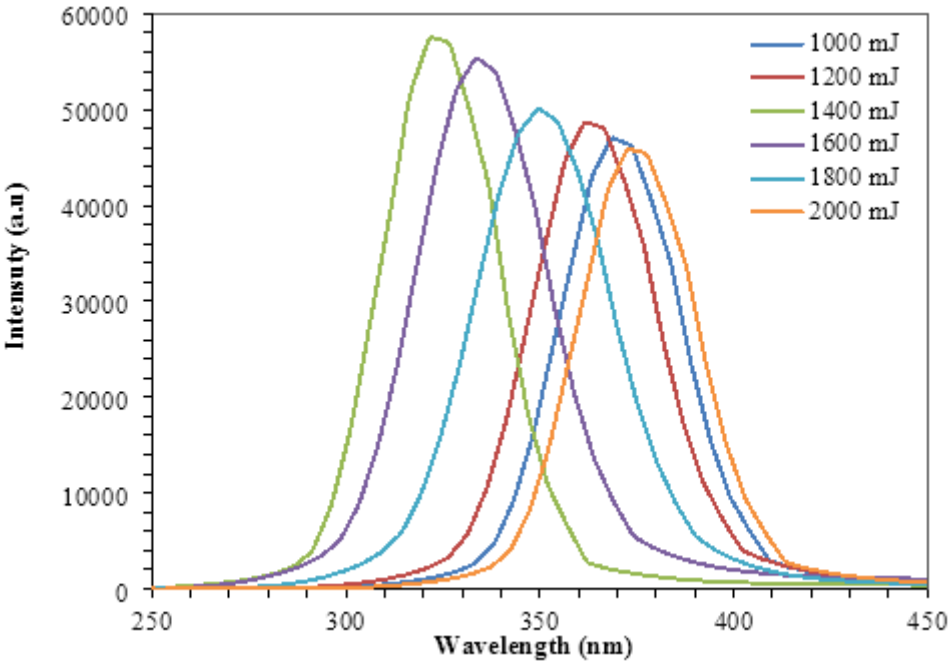

Figure 10

PL spectra of GaN at different ablation energies